Journal of Medicinal Chemistry

Article

Non-covalent Inhibitors of Mosquito Acetylcholinesterase 1 with Resistance-Breaking Potency

Sofie Knutsson, Cecilia Engdahl, Rashmi Kumari, Nina Forsgren, Cecilia Lindgren, Tomas Kindahl, Stanley Kitur, Lucy Wachira, Luna Kamau, Fredrik J. Ekström, and Anna Linusson

J. Med. Chem., **Just Accepted Manuscript** • DOI: 10.1021/acs.jmedchem.8b01060 • Publication Date (Web): 19 Oct 2018

Non-covalent Inhibitors of Mosquito Acetylcholinesterase 1 with Resistance-Breaking Potency

Sofie Knutsson,[1$] *Cecilia Engdahl,*[1$] *Rashmi Kumari,*[1] *Nina Forsgren,*[2] *Cecilia Lindgren,*[1] *Tomas Kindahl,*[1] *Stanley Kitur,*[3] *Lucy Wachira,*[3] *Luna Kamau,*[3] *Fredrik Ekström,*[2*] *and Anna Linusson*[1*]

[1]Department of Chemistry, Umeå University, SE-901 82 Umeå, Sweden

[2]Swedish Defence Research Agency, CBRN Defence and Security, SE-906 21 Umeå, Sweden

[3]Centre for Biotechnology Research and Development, Kenya Medical Research Institute, Nairobi, Kenya

$These authors contributed equally

*Corresponding authors. E-mail addresses: anna.linusson@umu.se; fredrik.ekstrom@foi.se

ABSTRACT

Resistance development in insects significantly threatens the important benefits obtained by insecticide usage in vector control of disease-transmitting insects. Discovery of new chemical entities with insecticidal activity is highly desired in order to develop new insecticide candidates. Here, we present the design, synthesis, and biological evaluation of phenoxyacetamide-based inhibitors of the essential enzyme acetylcholinesterase 1 (AChE1). AChE1 is a validated insecticide target to control mosquito vectors of e.g. malaria, dengue, and Zika virus infections. The inhibitors combine a mosquito versus human AChE selectivity with a high potency also for the resistance-conferring mutation G122S; two properties that have proven challenging to combine in a single compound. Structure-activity relationship analyses and molecular dynamics simulations of inhibitor-protein complexes have provided insights that elucidate the molecular basis for these

properties. We also show that the inhibitors demonstrate *in vivo* insecticidal activity on disease-transmitting mosquitoes. Our findings support the concept of non-covalent, selective, and resistance-breaking inhibitors of AChE1 as a promising approach for future insecticide development.

INTRODUCTION

The widespread usage of insecticides for control of disease-transmitting mosquitoes (vectors) has had a profound effect on the prevention of malaria, dengue, and Zika virus infections. The positive impact of these interventional public health measures is manifested in the hundreds of millions of averted malaria cases in sub-Saharan Africa over the last 15 years.[1] However, the intense use of insecticides has led to the development and spread of resistant mosquitoes to such an extent that resistant strains have now been identified against all major classes of insecticides recommended for vector control by the World Health Organization (WHO).[2] Furthermore, many of the currently used insecticides lack specificity for the vector over other non-target species,

which can have devastating effects on both humans and beneficial insects such as the pollinators.[3-5] Encouragingly, two agricultural insecticides re-purposed for vector control use have recently been prequalified by the WHO.[6]

The insecticides most commonly used for vector control disrupt the insect's nervous system by inhibiting voltage-gated ion channels (pyrethroids and organochlorines) or by inhibiting the essential enzyme acetylcholinesterase (AChE) (organophosphates and carbamates). The physiological role of AChE is to terminate nerve signaling by rapidly hydrolyzing the neurotransmitter acetylcholine.[7] Generally, insects have two genes encoding AChE enzymes: *ace-1* and *ace-2*,[8] whilst there is only one gene in vertebrates. In mosquitoes, AChE1 is thought to be the main catalytic enzyme.[9-10] Recently, the crystal structure of AChE1 from the malaria-transmitting mosquito *Anopheles gambiae* (*Ag*AChE1, amino acid numbering has been adapted to correspond to *m*AChE without taking deletions or insertions into consideration throughout the text, see Experimental section for details) was reported.[11] Similar to AChEs from other species, the structure shows a deep and narrow gorge with the catalytic serine at the bottom of the active site (*i.e.* S202, corresponding to S203 in *Homo sapiens* AChE (*h*AChE)). The catalytic serine

is the target for covalent insecticides, both organophosphates and carbamates. Natural populations of mosquito species have acquired organophosphate and carbamate resistance-conferring mutations in the *ace-1* gene.[10, 12-13] These mutations often occur close to, or within the active site gorge; the most widespread mutation in disease-transmitting mosquitoes is G122S in AChE1 of the *Anopheles* and *Culex* mosquitoes (corresponding to G122S and G119S in *h*AChE and *Torpedo californica* AChE, respectively).[10] The crystal structure of G122S-*Ag*AChE1 has recently become available, which show high similarity to the *Ag*AChE1 structure.[14] So far, it has proven challenging to develop inhibitors that combine a potency for G122S-*Ag*AChE1 with a mosquito versus human selectivity.[15-16]

Current design strategies for novel insecticides include covalent inhibitors that target either the catalytic serine residue (S202)[15-23] or the cysteine residue (C289) of AChE1.[24-28] As an alternative to inhibitors that react covalently with AChE1, we aim to develop *non-covalent* (non-bonding) inhibitors that offer the possibility to form important interactions with residues distant from the evolutionary conserved catalytic triad and the surrounding residues. We have recently discovered a number of non-covalent inhibitors that

selectively target AChE1 of the mosquitoes *An. gambiae* and *Aedes aegypti* (*Ae. aegypti*, transmitting dengue, chikungunya, and Zika virus infections).[29-30] Our research revealed that the inhibitor preferences for mosquito and human AChEs were distinctly different; only 10% of the found AChE inhibitors had a similar potency for human and mosquito AChEs. This finding is also consistent with our studies on AChE substrate preferences and kinetics comparing mosquito, mouse (*Mus musculus*, *m*AChE), and human AChEs.[31] One of the discovered compounds, the phenoxyacetamide-based compound **1** (Figure 1), was not only a potent inhibitor of the mosquito AChE1 *and* selective versus *h*AChE, but also a potent inhibitor of G122S-*Ag*AChE1 (Table 1).[29] Herein, we report the design, synthesis, *in vitro*- and *in vivo* evaluation of phenoxyacetamide-based analogues of **1**. The aim was to explore the molecular basis for the inhibitors' selectivity for mosquito AChE1 versus *h*AChE and their potency on G122S mutated *Ag*AChE1. Using a combination of X-ray crystallography (*m*AChE) and molecular dynamics (MD; mosquito AChE1s and *m*AChE) simulations, we provide a structural understanding of these potent and selective inhibitors of mosquito AChE1s.

RESULTS

Design and synthesis of mosquito AChE1 inhibitors

A set of 20 phenoxyacetamide-based compounds was designed based on **1** to explore the structure-activity relationships (SARs) for inhibition of mosquito AChE1 and *h*AChE (Figure 1 and Table 1). Three structural elements of **1** were investigated (Figure 1a); the importance of the ethylpiperazine group (A), the influence of the piperidine linker (B), and the effect of the biphenyl moiety (C). These three structural elements showed specific interactions with AChE in the **1**•*m*AChE crystal structure (Figure 1b) and a similar interaction pattern in the **1**•AChE1 homology models.[29] Fragment A interacts with residues in the catalytic site (CAS, mainly W86), fragment B is positioned between the phenols of Y124 and Y341 and C is positioned at the entrance of the active site gorge close to W286 (Figure 1). The new compounds were designed to investigate how changes of the interaction pattern of **1** affect the inhibition of AChEs (Table 1). Fragment A was removed or changed to a smaller piperazine or to tertiary amines with various electronic properties. The piperidine linker (fragment B) was changed to a more flexible propyl chain, and the distal phenyl group of fragment C was changed for other aromatic

groups or by exchanging the phenyl to an iodide. In the design of fragment C, the intention was also to improve the compounds' solubility in acetone, necessary for *in vivo* mosquito experiments.

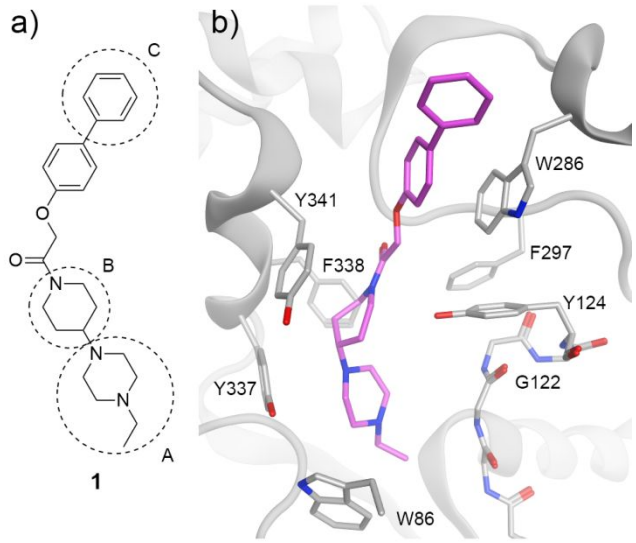

Figure 1. The chemical structure of **1** (a) and the binding pose of **1** in *m*AChE (b).[29] Three elements (A, B and C) of the parent molecule were varied in the design of analogues. Amino acid residues of *m*AChE that form the active site gorge are highlighted.

Synthesis of AChE inhibitors

The truncated piperidine analogue **2** and the morpholino- and *N*-ethylpiperazine analogues (**3** and **4**), which are lacking the piperidine linker, were obtained from **22** after amide formation (Scheme 1). Amines and diamines with rigid (**5** and **6**) or flexible (**8**, **9**, and **10**) linkers were prepared in an analogous fashion (Scheme 1). The synthesis of the rigid morpholino analogue **7** was accomplished by reacting 4-morpholinopiperidine **23** with chloroacetyl chloride to give amide **24**, which was substituted with 4-phenylphenol yielding the target compound (Scheme 2). The Suzuki coupling reaction was utilized to synthesize different para-substituted aryl ethers (**15**–**19** and **21**). For this purpose, 4-iodophenoxyacetic acid was converted to the acid chloride and coupled with various amines to produce the iodoaryl compounds **11**–**14** (Scheme S1). Suzuki coupling with 4-methoxyphenylboronic acid proceeded smoothly for the target compounds **17** and **18**. Due to synthetic problems related to solubility issues and low yields, **15** and **16** were produced using a variation of the route, with a reversed order of the Suzuki coupling and amide bond formation (Scheme S2). The analogues of **1** with structural variation on the distal aromatic ring were obtained in a similar manner, where two different aromatics were coupled to the iodoarene to give **19** and **21** (Scheme S3). Finally, compound **20**, where

the distal phenyl group of **1** is substituted for a cyclic ketone, was accessed from 5-hydroxy-1-indanone (Scheme S4). Several of the analogues had improved solubility in both water and acetone compared to **1**.

Scheme 1. Synthesis of compounds **2–6** and **8–10**.[a]

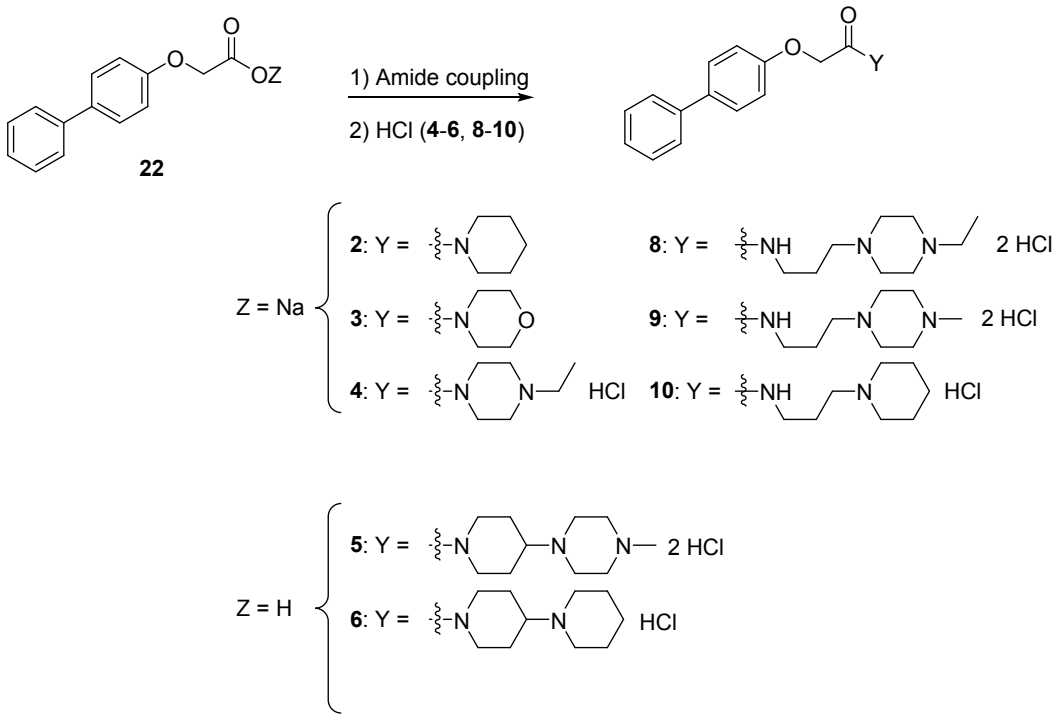

[a]For details, see Supporting Information.

Scheme 2. Synthesis of compound **7**.[a]

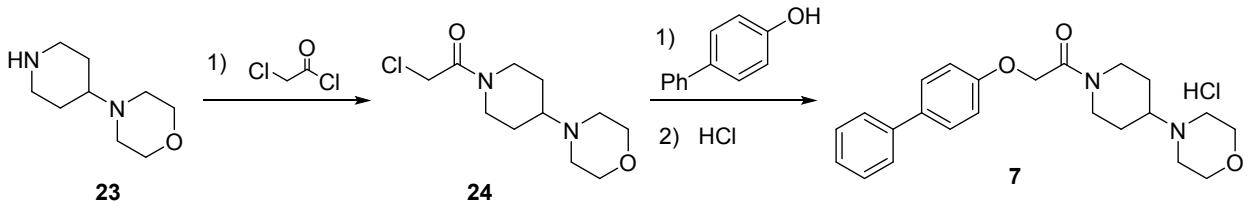

[a] For details, see Supporting Information.

Potency of AChE inhibitors

The potency of the synthesized phenoxyacetamide-based compounds (**2**–**21**) was evaluated by determination of their half-maximum inhibitory concentration (IC_{50}) values for *Aa*AChE1, *Ag*AChE1, the insecticide resistant mutant G122S-*Ag*AChE1, and *h*AChE (Table 1 and Figure S1).

The wild type mosquito enzymes showed similar inhibition profiles when comparing their IC_{50} values, and both enzymes are henceforth collectively referred to as AChE1. Importantly, also G122S-*Ag*AChE1 followed a similar trend and showed a similar sensitivity as the wild type enzyme. These findings differentiate the phenoxyacetamide-based compounds from our previous reported thiourea-based inhibitors that showed low potency on the resistance-conferring mutant.[30] Five compounds (**5**, **15**, and **19**–**21**) had sub-micromolar IC_{50} values for inhibition of all three mosquito enzymes. The

ethylpiperazine fragment (A) was proven crucial for an inhibitory effect; deletion of this fragment resulted in loss of activity (**2**). Modification of the resulting piperidine to a morpholine (**3**) or an ethylpiperazine (**4**) did not restore the potency. A small modification of fragment A to methylpiperazine (**5**) was tolerated, resulting in sub-micromolar IC_{50} values, while an exchange to a piperidine (**6**) or a morpholine (**7**) led to a reduction in potency (10- and 1000-times higher IC_{50} values, respectively). Also, the introduction of a flexible propyl linker instead of the piperidine as fragment B (**8**–**10** and **16**–**18**) led to loss of potency for all enzymes compared to the effects of their corresponding analogues. Modifying fragment C from a biphenyl to a 4-iodophenyl (compounds **11**–**14**) resulted in a loss of potency, while other modifications of the biphenyl ring (**15** and **19**–**21**) resulted in highly potent inhibitors, showing the importance of the aromatic ring at this position. The 4'-methoxybiphenyl (**15**) led to sub-micromolar potency on all three mosquito enzymes, and had a similar inhibition profile as the parent compound **1**. The other phenyl substituents, in combination with the piperidine-piperazine moiety (compounds **19**–**21**), also resulted in sub-micromolar inhibition of both AChE1 and G122S-*Ag*AChE1.

Table 1. Chemical structures and biochemical evaluation of the phenoxyacetamide-based inhibitors **1–21.**

ID	Structure	IC_{50} (μM)[a]				SR[b]
		*Aa*AChE1	*Ag*AChE1	G122S-*Ag*AChE1	*h*AChE	
1	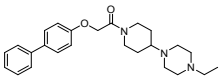	0.22 (0.12–0.38)	0.21 (0.12–0.37)	1.3 (0.81–2.0)	31 (29–34)	141
2	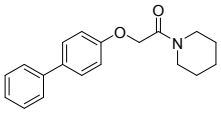	inactive[c]	inactive[c]	inactive[c]	inactive[c]	n.a.[d]
3	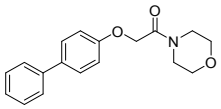	inactive[c]	inactive[c]	inactive[c]	inactive[c]	n.a.[d]

4	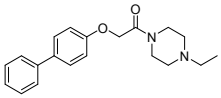	>200	>200	>200	>200	n.a.[d]
5	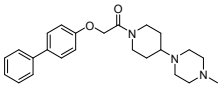	0.25 (0.24–0.26)	0.24 (0.19–0.32)	0.54 (0.34–0.86)	10 (8.4–13)	40
6	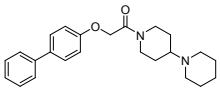	4.0 (2.5–6.4)	3.8 (3.5–4.2)	4.2 (3.2–5.4)	4.6 (3.4–6.3)	1.2
7	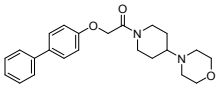	>200	>200	>200	93 (80–109)	n.a.[d]
8	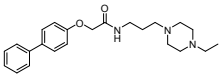	3.3 (3.1–3.5)	3.5 (3.2–3.9)	16 (13–21)	113 (93–136)	32
9	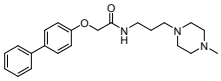	12 (11–12)	13 (11–14)	39 (33–46)	115 (96–136)	8.8

10	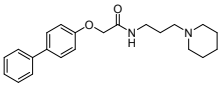	9.9 (6.5–15)	10 (7.6–13)	23 (19–29)	57 (49–66)	5.7
11	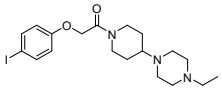	1.5 (1.3–1.7)	3.6 (2.6–5.0)	6.2 (5.1–7.4)	20 (18–23)	5.6
12	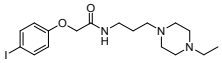	72 (27–190)	43 (19–97)	95 (74–123)	87 (74–101)	1.2
13	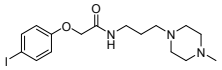	112 (100–126)	114 (101–128)	128 (104–157)	138 (106–180)	1.2
14	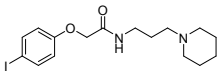	36 (28–46)	44 (37–53)	31 (23–42)	13 (13–14)	0.3
15	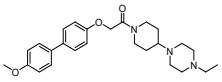	0.23	0.40	0.96	18	45

		(0.18–0.29)	(0.37–0.42)	(0.64–1.4)	(15–21)	
16	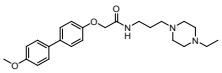	3.8 (3.7–4.0)	5.8 (4.8–7.0)	20 (17–24)	110 (98–124)	19
17	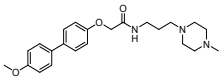	16 (15–17)	25 (24–27)	33 (13–80)	190 (116–316)	7.6
18	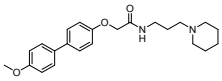	3.9 (3.7–4.1)	4.5 (3.7–5.5)	5.2 (3.7–7.3)	14 (13–15)	3.1
19	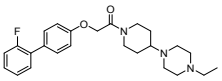	0.22 (0.18–0.26)	0.24 (0.10–0.59)	0.71 (0.56–0.90)	19 (15–23)	79

20	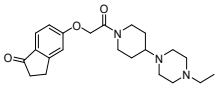	0.20 (0.18–0.22)	0.29 (0.24–0.35)	0.38 (0.34–0.42)	4.9 (4.3–5.5)	16
21	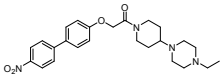	0.11 (0.096–0.13)	0.08 (0.069–0.093)	0.13 (0.11–0.15)	2.1 (1.4–3.2)	19

[a] 95% confidence interval given in parentheses; [b] SR = selectivity ratio, computed by taking the compound's IC_{50} value for *h*AChE and dividing by the higher of its IC_{50} values for *Ag*AChE1 or *Aa*AChE1; [c] Inactive at 1 mM; [d] n.a. = not applicable

In general, the compounds had a lower potency on *h*AChE than on the mosquito enzymes. For example, some of the most potent inhibitors of AChE1 and G122S-*Ag*AChE1 (**5**, **15** and **19**) showed at least 40 times greater IC_{50} values for the human enzyme. Interestingly, *h*AChE showed a different SAR compared to the mosquito enzymes. The exchange of fragment A from ethylpiperazine to a piperidine (**6** versus **1**)

that led to a decrease of potency for the mosquito enzymes, resulted in an increased potency on *h*AChE and consequently a complete loss of selectivity. Furthermore, modifying fragment C from a biphenyl to a 4-iodophenyl (compounds **11**–**14**) resulted in loss of selectivity, mainly due to lower inhibition of the mosquito AChE1s. In fact, **14** with 4-iodophenyl in combination with a flexible linker and a piperidine resulted in the strongest inhibition of *h*AChE and a reversed selectivity ratio (SR) of 0.3.

Structure-based analysis of the potency and selectivity of phenoxyacetamide-based compounds

A combination of X-ray crystallography, structural modelling, and MD simulations was used to elucidate the interactions and dynamics that govern the potency and selectivity of the phenoxyacetamide-based compounds. The inhibitors **15** and **10** were analyzed in complex with *Ag*AChE1 (**15** and **10**), G122S-*Ag*AChE1 (**15**), *Aa*AChE1 (**15**) and *m*AChE (**15** and **10**). Note that *h*AChE and *m*AChE are very similar in sequence and 3D structure and the compounds showed similar potency on *m*AChE compared to *h*AChE; the IC_{50}

values were 29 μM and 18 μM for **15**, and 61 μM and 57 μM for **10**, on *m*- and *h*AChE respectively (Figure S2).

Structures of phenoxyacetamide-based compounds in complex with mAChE and AChE1s. Using X-ray crystallography, the crystal structures of the **15**•*m*AChE (PDB code 6FSE) and **10**•*m*AChE (PDB code 6FSD) complexes were both determined to a resolution of 2.7 Å (Table S1). The electron density maps showed that **15** and **10** span the entire active site gorge of *m*AChE in a similar extended conformation as previously reported for **1** (PDB code 5FUM)[29], with the compounds forming interactions with W286 and W86 at the rim and the base of the gorge, respectively (Figure S3). The position and geometry of the inhibitors suggest that the carbonyl oxygen of **15** forms a water-bridged hydrogen bond with the backbone amide nitrogen of F295 while the carbonyl oxygen of **10** participates in a direct hydrogen bond with the same amide. Both complexes lack electron density for the distal, solvent exposed phenyl ring (fragment C) and this structural element has therefore not been modelled in the final structures. Detailed structural descriptions of **15**•*m*AChE and **10**•*m*AChE are available in the Supporting Information. Using the experimentally determined structures of **15**•*m*AChE, **10**•*m*AChE, and

*Ag*AChE1 (PDB code 5X61)[11] as templates, the **15**•*Aa*AChE1, **15**•*Ag*AChE1, **15**•G122S-*Ag*AChE1 and **10**•*Ag*AChE1 complexes were modelled and used as starting structures in the MD simulations.

*Molecular dynamics of **15**•AChE1 and **15**•mAChE complexes.* The conformational landscapes of the **15**•*m*AChE, **15**•*Aa*AChE1, **15**•*Ag*AChE1, and **15**•G122S-*Ag*AChE1 complexes were sampled by three 200 ns equilibrium MD simulations (S1–S3) for each complex. Based on the root mean square deviation (RMSD; Figure S4) the simulations were considered to be equilibrated after 50 ns, and thus subsequent analyses were made using the last 150 ns of each simulation. All enzymes were stable throughout the simulations with only small backbone structural deviations from the starting conformation (<2Å, Figure S4). In the simulations of the AChE1 complexes, the inhibitor **15** retained its binding pose with deviations < 4Å from the starting structures in all three simulated trajectories for each of the three mosquito enzymes (Figures 2a–c and 3a-c). Interestingly, **15** behaved differently in complex with *m*AChE, as large differences in the dynamics were observed compared to the mosquito complexes (Figure 2d), and three different local energy minima binding conformations were identified (Figure 3d-f). The second most

populated conformation of **15** in **15•***m*AChE was similar to the crystal structure (Figure 3e), while the other two showed large structural deviations compared to the crystal structure, mainly in the biphenyl part of the inhibitor that interacts with residues at the entrance of the gorge.

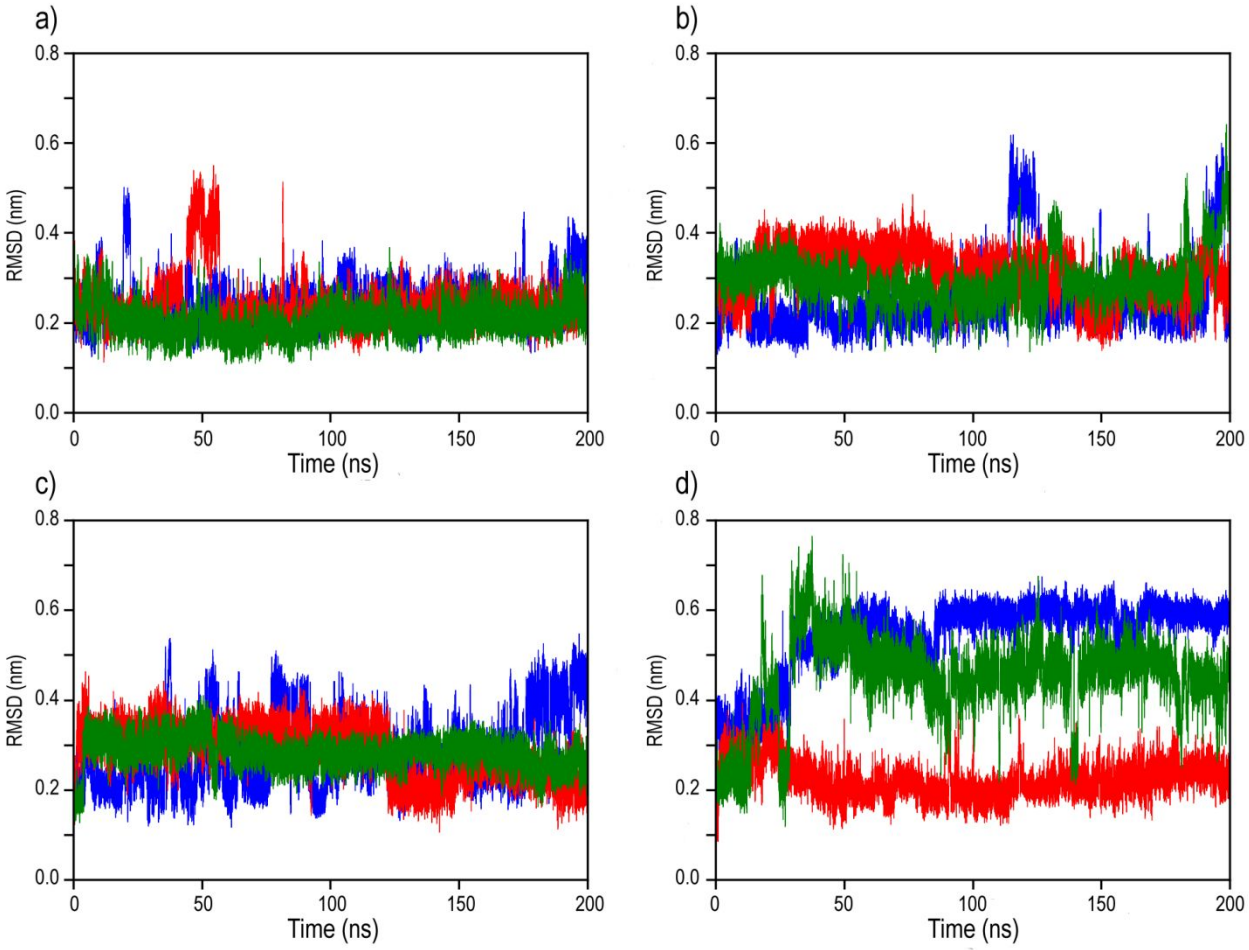

Figure 2. The dynamics over time of compound **15** in complex with a) *Aa*AChE1, b) *Ag*AChE1, c) G122S-*Ag*AChE1, and d) *m*AChE according to its RMSD after

superimposing the enzyme backbone; blue, red, and green curves correspond to simulations S1, S2, and S3, respectively.

*Interaction patterns between **15** and the enzymes.* Contact frequencies between **15** and residues in the binding sites were calculated to investigate the positioning of **15** in the AChEs throughout the simulations. For all AChE complexes, the inhibitor had substantial contacts with amino acid residues Y335/Y341 (mosquito residue numbering/mouse residue numbering) and W87/W86 throughout the entire simulations (Figure S5). Notably, differences in the contacts for the **15**•AChE1 complexes compared to **15**•*m*AChE were observed. In the AChE1 complexes, **15** had frequent contacts also with residues Y331 and F332 at the CAS while the corresponding contacts in **15**•*m*AChE (Y337 and F338) were infrequent. At the entrance of the gorge, **15** had frequent contacts with residue W283/W286, although it was less frequent in *Ag*AChE1 and *m*AChE compared to *Aa*AChE1 and G122S-*Ag*AChE1. This was due to flipping of the W283 indole towards the exterior solvent in one of the parallel simulations in *Ag*AChE1, while in the case of

*m*AChE, the biphenyl group was more dynamic resulting in fewer contacts with W286 (Figures 3e-f and S5b and d).

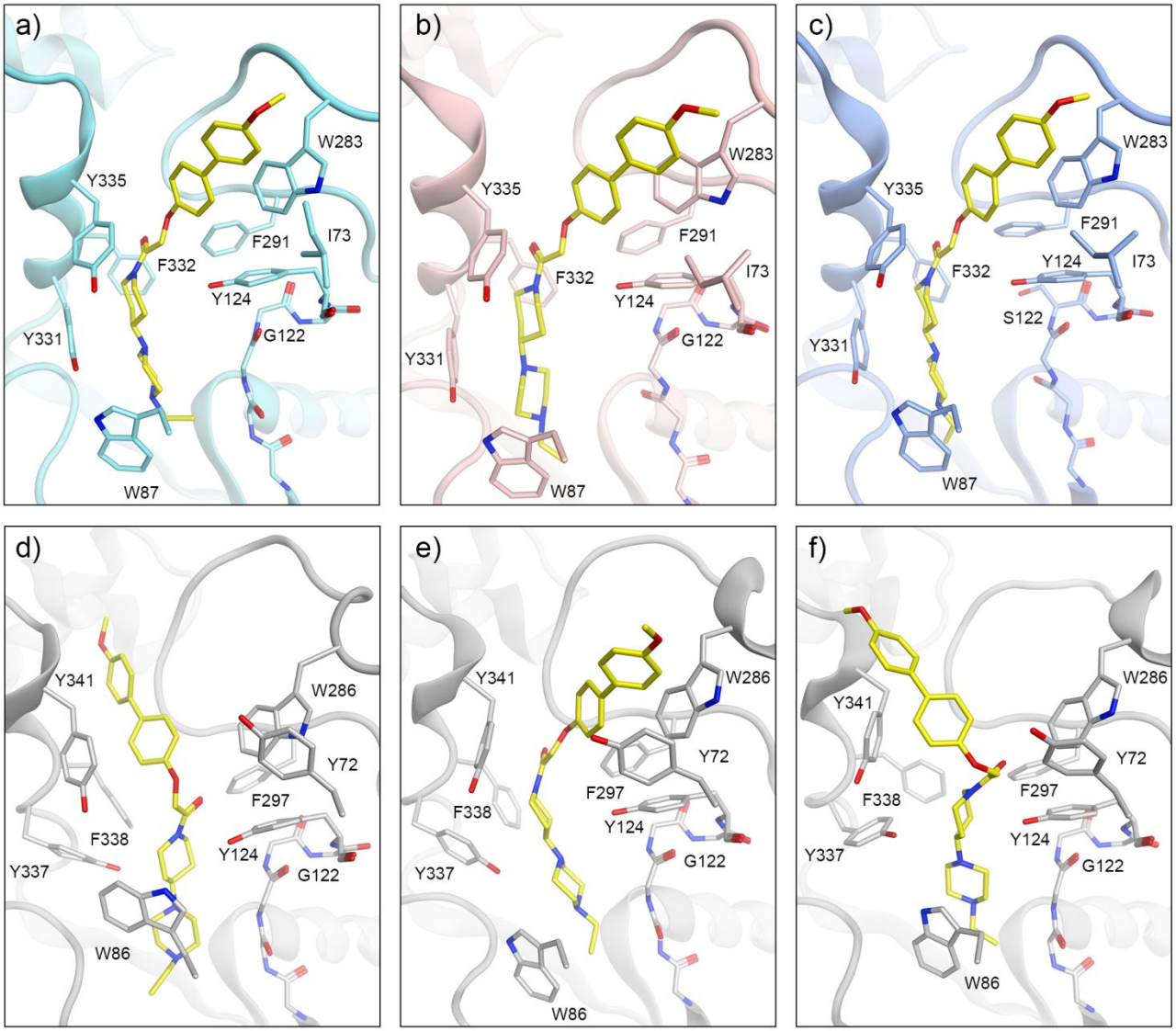

Figure 3. Binding poses of **15** in AChEs based on MD simulations. The poses were extracted from the most populated conformations of **15** (yellow) during the MD simulations

of the mosquito enzymes *Aa*AChE1 (a, cyan), *Ag*AChE1 (b, pink), and G122S-*Ag*AChE1 (c, blue). The three most populated conformations of **15** in the mouse enzyme (grey) are shown in d–f, where e is most similar to the crystal structure of **15**•*m*AChE.

The binding strengths between **15** and the residues of the identified contacts were assessed by decomposing calculated binding energies between **15** and AChEs for different complexes per amino acid residue using the molecular mechanics/Poisson-Boltzmann surface area (MM/PBSA) method (Table 2; see Methods for details). The energy values show that the binding strengths between **15** and residues Y335/Y341 and W87/W86, respectively, were strong in all enzymes suggesting that these interactions anchor **15** in all the AChEs in a similar fashion (Table 2).

The contact analyses revealed differences between the binding poses of **15** in the AChE1s and *m*AChE, where **15** had more frequent contacts in the CAS with Y331 and F332 in AChE1 as compared to in *m*AChE. The binding energy decomposition showed that the piperidine fragment of **15** formed strong binding interactions with the aromatic ring of Y331 throughout the simulations of the mosquito enzymes. The corresponding

interaction in **15**•*m*AChE (**15**•Y337) showed only weak binding strengths. Moreover, the interactions between **15** and F332/F338 appear to be of medium strengths and approximately similar for all complexes, showing that differences in contact frequencies do not directly translate into differences in binding strengths. At the entrance of the gorge, stronger binding contributions were seen between **15** and residues W283 and I73 of AChE1 compared to corresponding interactions in **15**•*m*AChE (W286 and Y72). Taken together, the weaker interactions in *m*AChE resulted in large mobility of **15** in the entire binding site in general and at the entrance in particular (Table 2 and Figures 2 and 3).

Analyses of contact frequencies of **15**•G122S-*Ag*AChE1 and minimum distance calculations between **15** and S122 (Figures S5c and S6) showed that there were no substantial contacts between **15** and S122 during the simulations. The strong binding strengths between **15** and the amino acid residue Y331 contributed to binding poses of **15** distant to the mutation site at position 122 of the mosquito enzyme (Table 2). This resulted in sufficient space in **15**•*Ag*AChE1 to accommodate the G122S mutation without interrupting the binding of **15**. These observations explain the high potency of **15** for G122S-*Ag*AChE1 (Table 1).

*Molecular dynamics of the **10**•AgAChE1 complex.* To further elucidate the forces governing the inhibitor potency, complex **10**•*Ag*AChE1 was simulated and analyzed in parallel with the studies of **15**•*Ag*AChE1. Compared to **15**, inhibitor **10** has a substantially different chemical composition of the fragments interacting with amino acid residues in the binding site of the AChEs, *i.e.* the ethylpiperazine (fragment A) and piperidine (fragment B) moieties of **15** have been replaced by a piperidine moiety and a flexible propyl chain in **10** (Table 1). These chemical modifications resulted in an approximately 40 times higher IC_{50} value of **10** for *Ag*AChE1 compared to **15** (Table 1). The **10**•*Ag*AChE1 simulations were considered to be equilibrated after 50 ns according to the RMSD, and the enzyme was stable throughout the simulations (Figure S7). Inhibitor **10** was more dynamic compared to **15** in the binding site of *Ag*AChE1 (Figure S8). The contact frequency analysis of **10**•*Ag*AChE1 showed that **10** had frequent contacts with the same residues found to substantially contribute to binding of **15** (listed in Table 2 and Figure S9). However, the decomposition of the binding energy between **10** and *Ag*AChE1 revealed that the interactions between **10** and amino acid residues in the binding site were considerably weakened compared to **15**•*Ag*AChE1 (Table 2). In particular, the

binding strengths between **10** and the residues W87, Y331, and F332 were significantly reduced, highlighting the importance of the interactions between **15** and these residues (Table 2). It appears that the chemical differences between **10** and **15** resulted in the weaker interactions of **10** with amino acid residues F332, Y331, and W87 thus making **10** more dynamic (Figures S8 and S10), which altogether contributed to the loss of inhibitory potency compared to **15**.

Table 2. Energy contribution of interactions between individual residues and inhibitors to total binding energy.

Residues	**Energy contribution to binding (kJ/mol)[a]**				
mosquito/mouse	**15**•*Aa*AChE 1	**15**•*Ag*AChE 1	**15**•G122S-*Ag*AChE1	**15**•*m*AChE	**10**•*Ag*AChE 1
W283/W286	**-12.0±0.5**	-7.8±0.9	**-11.0±0.5**	-6.1±0.8	**-9.5±0.7**

I73/Y72	-2.8±0.3	-5.1±0.5	-4.4±0.6	-3.6±0.5	-3.1±0.3
F291/F297	-4.3±0.2	-3.6±0.3	-3.6±0.3	-3.0±0.3	-3.3±0.3
Y335/Y341	**-13.2±0.3**	**-13.7±0.4**	**-14.0±0.3**	**-11.7±0.5**	**-11.1±0.4**
Y124/Y124	-3.1±0.3	-2.8±0.3	-2.5±0.2	-2.8±0.4	-4.5±0.3
Y331/Y337	**-11.5±0.4**	**-9.4±0.5**	**-11.2±0.4**	-3.8±0.3	-7.3±0.5
F332/F338	-8.0±0.3	-7.0±0.3	-6.8±0.5	-6.1±0.6	-5.4±0.4
W87/W86	**-10.4±0.3**	**-10.5±0.5**	**-10.7±0.5**	**-12.6±0.5**	-7.7±0.4

[a]The energy of contribution was calculated by decomposing binding energy using MM/PBSA method with solute dielectric constant of eight. Residues with less than -4 kJ/mol in at least one of the complexes were considered for the comparison.

Insecticidal effects of phenoxyacetamide-based AChE1 inhibitors on mosquitoes

The improved solubility in acetone and mosquito saline of the designed compounds compared to parent compound **1** enabled us to evaluate *in vivo* potency of selected

phenoxyacetamide-based analogues. The intrinsic insecticidal efficacy of inhibitors **19–21** was investigated by topical application on adult female *Ae. aegypti* and *An. gambiae* mosquitoes (Figure 4).

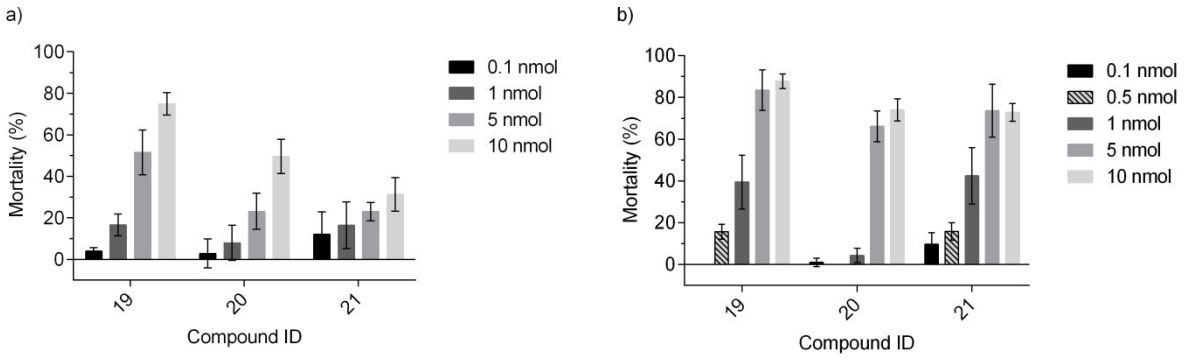

Figure 4. The intrinsic insecticidal efficacy of compound **19-21** recorded 24 hours after topical application on adult female *Ae. aegypti* (a) and *An. gambiae* (b) mosquitoes.

All three inhibitors showed insecticidal activity where the 2'-fluorobiphenyl compound **19** had the highest *in vivo* potency; a dose of 10 nmol/mosquito (4.26 µg/mosquito) killed 75% and 88% of adult *Ae. aegypti* and *An. gambiae* mosquitoes, respectively. The mortality rates for **20** and **21** were lower when applied to *Ae. aegypti* mosquitoes (50% and 31%, respectively), while only a slight decrease in mortality compared to **19** was observed when applied to *An. gambiae* mosquitoes (Figure 4 and Table S3–S4). In all

experiments, the mortality rates after 48 h were on average 5% higher compared to mortality rates at 24 h. Overall, the *Ae. aegypti* mosquitoes appeared less affected by the compounds in comparison to the more sensitive *An. gambiae* mosquitoes, a trend also seen for our previously reported thiourea-based AChE1 inhibitors[30] and other covalent inhibitors.[19] The estimated LD_{50} of inhibitor **19** on adult *Ae. aegypti* (2.13 μg/mosquito) is approximately 400 and 1200 times higher compared to that of the carbamate insecticides propoxur (LD_{50} = 0.0054 μg/mosquito) and bendiocarb (LD_{50} = 0.0018 μg/mosquito), respectively.[19] It was also noted that all three of the tested compounds exhibited lower than expected mosquitocidal activity based on their AChE1 IC_{50} values; such discrepancies have also been experienced previously by us[30] and others.[16, 18, 21] To investigate the marked difference between *in vitro*- and *in vivo* potency, selected phenoxyacetamide-based analogues and the insecticide propoxur were injected into live *Ae. aegypti* mosquitoes. Injections of 0.115 nmol/mosquito (ca 56 ng/mosquito) of the same set of compounds (**19**–**21**) and an additional compound (**5**) directly into *Ae. aegypti* females resulted in 55–64% mortality. The doses required for equivalent mortality after topical administration were 40 times higher for **19** and over 80 times higher for **20** and **21**.

Injections of propoxur (0.099 nmol/mosquito; 21 ng/mosquito) killed 85% of the mosquitoes (see Supporting Information), showing that the difference in *in vivo* potency between the developed inhibitors and propoxur was smaller when the compounds were injected into the mosquito compared to applied topically. The differences in mortality between topical administration and microinjections of the compounds indicate that the observed lower-than-expected *in vivo* efficacy of these compounds was, at least partly, due to poor penetration over the exoskeleton (Table 3 and Table S5). The microinjection results also revealed that the differences in *in vivo* potency between the three compounds after topical application were due to differences in penetration abilities since no difference in insecticidal activities could be observed after direct injection of the compounds.

Table 3. Insecticidal effect of phenoxyacetamide-based inhibitors by microinjections into female *Ae. aegypti* mosquitoes.

Compoun	Dose	Mortality (%)

d	(ng)	(nmol)	24 h	48 h
5	53.6	0.115	58	66
19	57.3	0.115	55	56
20	52.7	0.115	58	64
21	60.4	0.115	64	69

DISCUSSION

The phenoxyacetamide-based inhibitors have a good shape complementarity to the entire active site gorge of AChEs, forming non-covalent interactions with several amino acid residues at the bottom of the active site and all the way up to the entrance of the gorge. The SARs between the set of inhibitors and AChE1 or *h*AChE, respectively, showed a clear species difference in inhibitor preferences, despite the high similarity in the 3D structures of *Ag*AChE1, *h*AChE, and *m*AChE. The different preference for non-covalent inhibitors between AChE1 and *h*AChE appears to be a general feature, as it has been shown for inhibitors identified in HTS[29] and for a SAR study of thiourea inhibitors.[30] The molecular dynamics studies were needed to provide insights regarding the selectivity

and potency of the submicromolar phenoxyacetamide-based AChE1 inhibitors; analyses of the static structures of AChEs in complex with the inhibitors did not reveal any distinct differences between the inhibitors' interaction patterns in AChE1 and *m*AChE. However, it was clear from the MD simulations that **15** had different behaviors in the active site gorges of AChE1 and *m*AChE, respectively. It has previously been discussed whether differences in amino acid sequences between mosquito and vertebrate enzymes' in two loops located at the entrance of the gorge could be responsible for the observed species selectivity of the non-covalent inhibitors.[29] We find no support for that hypothesis in the results from the MD simulations, rather it appears that it was interactions with amino acid residues in the cavity helix (residues 328 to 335 in mosquito/334 to 341 in mouse) that yielded the differences in potency. In the mosquito complexes, the piperidine (fragment B) and the acetamide of **15** had strong arene interactions with Y331 and Y335, respectively, which resulted in one major binding conformation of the inhibitor throughout the simulations. In contrast, **15** was highly dynamic in the complex with *m*AChE, and three substantially different binding conformations were identified. The second most populated cluster, which contained the conformation most similar to the crystal structure, was also

most similar to the binding conformation in the mosquito enzyme. The key difference here was the absence of arene interactions between **15** and Y337 in *m*AChE (Y331 in AChE1). In the MD simulations of inhibitor **10** (with a modified fragment B) in complex with *Ag*AChE1 the discussed arene interactions with Y331 could not be observed and the cluster analysis yielded dual binding poses (Figure S10), which could explain the 40 times higher IC_{50} value of **10** compared to **15**.

The phenoxyacetamide-based inhibitors were also potent on the resistant-conferring mutant G122S-*Ag*AChE1, which had a similar SAR as the wild type AChE1. Activity on G122S-*Ag*AChE1 has also been reported for other non-covalent AChE1-inhibitors,[31-32] including donepezil and compound C7653.[31] However, this does not appear to be a general property of non-covalent inhibitors[30]. Our MD simulations suggest that the strong arene interactions formed between the inhibitors and the tyrosine residues in the cavity helix of AChE1 yield a binding pose that allow for high potency also for the resistant conferring mutant G122S-*Ag*AChE1. Such interactions are also observed in crystal structures of AChEs in complex with both donepezil and C7653.[33-34] Unique for the phenoxyacetamide-based inhibitors is that they combine AChE1 vs. *h*ACHE selectivity

with a strong potency on the resistant-conferring mutant G122S-*Ag*AChE1, which is not the case for donepezil and C7653 that are more potent on *h*AChE than on AChE1.[29, 31]

The sub-micromolar phenoxyacetamide-based inhibitors showed insecticidal activity on both *Ae. aegypti* and *An. gambiae*. However, the compounds were less potent *in vivo* than would be expected considering their IC_{50} values. We hypothesize that this may be due to the presence of aliphatic amines in the inhibitors. Other insecticidal molecules presented by us[30] and others[35], which contain aliphatic amines have shown a discrepancy between the *in vitro* and *in vivo* potency, with a much lower insecticidal activity than expected. Retrospective studies of agricultural- and public health insecticides show that the current insecticides have a narrow physicochemical space, *i.e.* have limited chemical variations; it is significantly smaller than the physicochemical space of pharmaceutical drugs.[36-39] For instance, insecticides contain a significantly lower number of hydrogen bond donors, due to a low frequency of alcohols and amines. It has been suggested that aliphatic amines are absent in insecticides due to low bioavailability.[36-37, 39] When the inhibitors studied here were injected directly into the mosquitoes, the potency increased 40 to 80 times as compared to the topical application, showing that part of the difference

between *in vitro* and *in vivo* potency was due to penetration through the exoskeleton. We also note that in order to be able to compete with current carbamates used for IRS (*e.g.* bendiocarb),[19] the topical mosquitocidal activity of the compounds presented here needs to be improved ~1200 times. For efficient insecticidal candidates based on these inhibitors, future studies to improve the mosquitocidal activity could include improvements of compound delivery via formulation developments or further exploration of possible phenoxyacetamide-analogues without aliphatic amines.

CONCLUSIONS

We report the design, synthesis and biochemical evaluation of a set of phenoxyacetamide-based inhibitors of mosquito AChE1. Three of the analogues **5**, **15**, and **19** had a sub-micromolar potency for the wild type AChE1 proteins *and* the resistance-conferring mutant G122S-*Ag*AChE1 combined with a mosquito versus human selectivity (at least 40 times greater IC_{50} values for the human enzyme). The SAR proved to be similar for the mosquito AChE1s, while the SAR for *h*AChE was different, suggesting an opportunity to improve selectivity of AChE1 inhibitors even further. The MD simulations

suggest that strong interactions between the inhibitors and tyrosines at the cavity helix (Y331 and Y335) were responsible for the high potency on mosquito enzymes; these interactions were much weaker in *m*AChE. Importantly, a selection of AChE1 inhibitors (**19**-**21**) also showed insecticidal activity on the two mosquito species *An. gambiae* and *Ae. aegypti*, which had not been demonstrated for **1** due to its poor solubility in acetone and mosquito saline. Inhibitor **19** is considered the superior in the presented set of analogues due to its high mosquito versus human selectivity and demonstrated *in vivo* activity. In summary, our exploration of phenoxyacetamide-based inhibitors show that non-covalent inhibitors of mosquito AChE1 could provide a viable alternative in the discovery of new selective and resistance-breaking insecticide candidates to be used in vector control of disease-transmitting mosquitoes.

EXPERIMENTAL SECTION

Synthesis

General. All reactions were carried out under inert atmosphere (N_2) unless otherwise stated. THF and DMF were dried in a solvent drying system and freshly collected prior to

reaction (THF was passed through neutral alumina; DMF was passed thorough activated molecular sieves followed by an isocyanate scrubber). All microwave reactions were carried out in a monomode reactor using Smith process vials sealed with a Teflon septum and an aluminium crimp top. The temperature was measured with an IR sensor, and reaction times refer to the irradiation time at the target temperature. Reactions were monitored using TLC (silica gel matrix, layer thickness 200 µm, particle size 25 µm) with UV-detection (254 nm) or developed using $KMnO_4$ solution. Flash column chromatography (eluents given in brackets) was performed on normal phase silica gel (Merck, 60 Å, 40–63 µm). ^{1}H and ^{13}C NMR spectra were recorded on a Bruker DRX-400 or DRX-600 instrument at 298 K in $CDCl_3$ using residual $CHCl_3$ (δ_H = 7.26 ppm) or $CDCl_3$ (δ_C = 77.16 ppm) as an internal standard, $(CD_3)_2SO$ using residual $(CD_3)(CD_2H)SO$ (δ_H = 2.50 ppm) or $(CD_3)_2SO$ (δ_C =39.52 ppm) as an internal standard, or CD_3OD using residual CD_2HOD (δ_H = 3.31 ppm) or CD_3OD (δ_C = 49.0 ppm) as an internal standard. When $CDCl_3$:CD_3OD mixtures were used, CD_3OD was used as the internal standard, and when CD_2Cl_2:CD_3OD mixtures were used, CD_2Cl_2 was used as the internal standard using residual $CDHCl_2$ (δ_H = 5.32 ppm) or CD_2Cl_2 (δ_C = 53.84 ppm). LC-MS analyses were

performed on a Waters LC system using a Xterra MS C18 18.5 μm 4.6x50 mm column and an acetonitrile:water eluent system containing 0.2% formic acid. Eluting compounds were detected by monitoring the eluent's absorption (254 nm) and mass spectrometry was performed in positive ion mode using a Waters micromass ZG 2000 electrospray instrument. High-resolution mass spectrometry (HRMS) data was recorded on Agilent Technologies 6230 TOF LC/MS in ESI mode. The compounds used in the biological evaluations exhibited ≥95% purity by analytical HPLC analysis using a Nexera UHPLC system (Shimadzu, US) connected to a diode array detector (SPP M20A). The samples were analyzed using a Nucleodur C18 HTec column (EC 150 × 4.6, 5 μm, Macherey-Nagel) with a flow rate of 1 mL/min. Aliquots of 2 μL of each sample were injected and detection was performed at 254 nm. The mobile phase was composed of solvent A (H_2O with 0.1% TFA) and solvent B (acetonitrile with 0.1% TFA). The binary gradient profile with solvent B as the reference was as follows: 0−1.5 min, 10% B; 1.5−11.5 min, 10−100% B; 11.5−26.5 min, 100% B; 26.5−27 min, 100−10% B; 27−30.5 min, 10% B. Before first injection, the column was equilibrated at 10% B for 1.5 min. The description

of synthesis, purification, and structural determination of building blocks and the phenoxyacetamide-based analogues **2–21** is provided in the Supporting Information.

IC_{50} determinations

IC_{50} values for recombinant *Aa*AChE1, *Ag*AChE1, G122S-*Ag*AChE1,[31] and *h*AChE[40] were determined according to the following procedure. Freshly prepared stock solutions of the compounds were prepared from solid material in DMSO at a concentration of 100 mM. Working dilutions thereof were prepared in either 0.1 M sodium phosphate buffer (pH 7.4) or MilliQ water, depending on the solubility of the compounds. Compound solutions of eight different concentrations up to a maximum of 1 mM were used. The activity measurements were performed using secreted non-purified proteins in growth medium, and enzymatic activity was measured using the Ellman assay[41] adapted to a 96-well format. Liquid handling of buffer solution containing buffer, enzyme and reagent was performed using a QIAgility robotic benchtop instrument (Qiagen). Compounds were added manually and reaction was thereafter immediately started by addition of substrate using the FlexStation 3 Multi-Mode Microplate Reader (Molecular Devices). The assay

was performed at 30°C in a final assay volume of 200 µl of 0.1 M phosphate buffer (pH 7.4) containing 0.2 mM of the reagent 5,5′-dithiobis(2-nitrobenzoic acid) and 1 mM of the substrate acetylthiocholine iodide. The enzymatic reaction was measured by monitoring changes in the absorbance of individual wells at 412 nm over 60 s in the same FlexStation 3 Multi-Mode Microplate Reader as mentioned above. The average slope determined for eight positive (uninhibited) controls on each plate was taken to represent 100% activity and the activity observed in the sample wells were quantified in relation to this value. IC_{50} values were calculated using non-linear regression (curve fitting) in GraphPad Prism[42] and the log [inhibitor] versus response variable slope equation was fitted using four parameters. For all four targets, all compounds were tested at least twice at different time points and with newly prepared dilutions from solid material each replicate.

Generation, collection, and refinement of crystal structures

The crystallization of *m*AChE was performed as previously described.[43] Small amounts of the ligands **15** or **10** were added to a soaking solution consisting of 30% (v/v) polyethylene glycol 750 monomethylether in 100 mM HEPES buffer, pH 7.0 until

saturation was reached. The soaking solution was then added to a crystal of *m*AChE over approximately five minutes and the crystal was incubated for an additional few minutes prior to flash-freezing in liquid nitrogen. X-ray diffraction data was collected at the BESSY synchrotron (Berlin, Germany) using beam line MX 14-3 and at the MAXIII lab synchrotron (Lund, Sweden) using beam line I911-3. Images were collected using an oscillation angle of 0.1° per exposure. The intensity data were indexed and integrated using XDS[44] and scaled using Scala.[45] The structures were determined using rigid-body refinement starting with a modified *apo* structure of *m*AChE (PDB code 1J06[46]). The presence of the ligand in the binding site of the *m*AChE crystals was confirmed based on the initial $2|F_o|-|F_c|$ and $|F_o|-|F_c|$ omit maps. Further crystallographic refinement, as well as evaluation of the final model, was performed using the Phenix software suite[47] (Table S1). Several rounds of refinement were performed, alternating with manual rebuilding of the model after visualizing the $2|F_o|-|F_c|$ and $|F_o|-|F_c|$ electron density maps using COOT.[48] Simulated annealing omit maps, starting from the model where the coordinates for the ligands were omitted, were used to guide the modelling of the ligand.

Modelling of AChE1 complexes

The *Ag*AChE1 sequence was adapted to the *m*AChE numbering by subtracting 158 from the UNIPROT numbering (accession number: XP_321792; UNIPROT code: ACES_ANOGA). The model of *Ag*AChE1 in complex with **15** was obtained by aligning the two crystal structures **15**•*m*AChE (PDB code 6FSE, presented here) and *Ag*AChE1 (PDB code 5X61), and subsequently copying the coordinates of **15** from the **15**•*m*AChE PDB file into the PDB file of *Ag*AChE1. The model for *Ag*AChE1 mutant with the **15** was built by mutating the glycine 122 into serine in PyMOL using the modelled structure of **15**•*Ag*AChE1. The **15**•*Aa*AChE1 model were obtained by homology modelling using the *Ag*AChE1 crystal structure (PDB code 5X61) as a template. The amino acid sequence of *Aa*AChE1 (accession number: ABN09910) was aligned to the *Ag*AChE1 sequence (accession number: XP_321792; UNIPROT code: ACES_ANOGA) using Clustal Omega[49]. The sequences were edited both at N- and C-terminals based on the coordinates available in crystal structure of *Ag*AChE1. *Aa*AChE1 models were then generated using Modeller 9.18 version based on the alignment.[50] In total, 500 models were generated, and a few top models were selected for further processing based on the

Modeller DOPE score. The final model was selected based on analysis using PROCHECK, analysis of Ramachandran Plot and RMSD values. Compound **15** was modelled into the active site of the *Aa*AChE1 model using the same procedure as for **15**•*Ag*AChE1. The model of *Ag*AChE1 in complex with **10** was obtained following the same procedure as for **15**•*Ag*AChE1 using the crystal structure of **10**•*m*AChE (PDB code 6FSD, presented here) and *Ag*AChE1 (PDB code 5X61).

Molecular dynamics simulations

System Preparation. Parameter files for **15** were generated by extracting the coordinates from the crystal structure file of *m*AChE and hydrogen atoms were added using the Open-Babel package.[51] The distal (ethyl substituted) nitrogen of the piperazine fragment was protonated based on pK_a calculations. To generate partial atomic charges of **15**, at first, the geometry of the compound was optimized using HF/6-31G* basis set and the electrostatic surface potential (ESP) was calculated with Gaussian 09.[52] The ESP was used to calculate partial atomic charges using the restrain electrostatic potential (RESP) method within the antechamber program of AmberTools,[53] and subsequently the

general amber force field (GAFF) parameters[54] for the compound was generated. The AMBER topology/coordinate files were created using *parmchk* and *tleap* program of the AmberTools and the AMBER format files of **15** were converted to the GROMACS format using the acpype python script.[55]. Further, topology and coordinate files for AChEs of mouse and mosquito were generated using the AMBER99SB-ILDN force field[56] with *pdb2gmx* program of GROMACS package.[57] The coordinate and topology files of AChEs and **15** were merged to obtain the final starting structures and topology files for the complexes in case of **15**•*Ag*AChE1, **15**•G122S-*Ag*AChE1, **15**•*Aa*AChE1, and **15**•*m*AChE. Parameter and topology files for compound **10** were generated by the same procedure described above for **15**. The nitrogen of the piperidine fragment was protonated based on pK_a calculations. The final starting structure and topology files for the **10**•*Ag*AChE1 complex were generated similarly as above for **15**.

Simulation Setup. Equilibrium MD simulations of each prepared molecular system were performed using GROMACS-5.1.2. The complex was placed in the centre of a dodecahedron periodic box, subsequently solvated by addition of water molecules and neutralized by the addition of 0.150 M of NaCl. The TIP3P water model[58] was used in the

simulations. The energy of the molecular system was minimized using the steepest descent algorithm. The molecular system was heated to 300 K during the 100 ps NVT simulation with 2 fs time step. The pressure was then equilibrated to 1 atm during 500 ps NPT simulation with 2 fs time step. In both simulations, all heavy atoms were restrained at starting positions with the force constant of 1000 kJ mol^{-1} nm^{-2}. The restraint was gradually removed during a simulation of 1 ns time period with 2 fs time step. In all these simulations both temperature and pressure was regulated using the Berendsen algorithm.[59] In the next step, three parallel production simulation runs were performed for 200 ns with 2 fs time step with different initial velocities. The temperature and pressure was maintained at 300 K and 1 atm using the v-rescale temperature and Parrinello-Rahman pressure coupling method.[60-61] The time constants for the temperature and pressure coupling were kept at 0.1 and 1 ps, respectively. The short range non-bonded interactions were computed for the atom pairs within the cut-off of 1.4 nm, while the long range electrostatic interactions were calculated using Particle-Mesh-Ewald summation method with fourth-order cubic interpolation and 1.2 Å grid spacing.[62] All bonds were constrained using the parallel LINCS method.[63-64]

Analysis. RMSD values were calculated using the *gmx rms* module of GROMACS using the starting structure as the reference. The RMSD of compound **15** with reference to its starting position was calculated after superimposing enzymes backbone To analyse the most populated binding pose/s of **15** during the simulations, the conformations from the combined three trajectories were clustered using Jarvis-Patrick algorithm with 0.1 nm RMSD cut off after superimposing enzyme backbone to starting structure. The differences in interaction pattern between **15** in *Ag*AChE1, *G*1*22S*-*Ag*AChE1, *Aa*AChE1, and *m*AChE were studied by contact maps and calculation of binding energy contribution. To generate the contact maps, the *g_distMat* module was used with a distance cut-off of 4 Å. A residue was defined as a contact residue if any atom of that residue remain within 4 Å of the compound for at least 60% of the simulation time in at least one of the parallel simulations. For quantifying the significance of these contacts, the binding energetic contribution of each residue to the binding of **15** was calculated using the tool *g_mmpbsa*.[65-66] The tool uses MM-PBSA method for calculating binding energy and the energy is further decomposed as a function of residues to get the contribution of each residue. Those residues whose binding energy contribution was < -4 kJ/mol were considered for

analysing the differences in the interaction pattern in mouse and mosquito. Interactions with charged residues were discarded due to uncertainties in the calculation method.

In vivo experiments

Ae. aegypti Mombasa strain and *An. gambiae* Kisumu strain from Kenya, both susceptible to commercial insecticides, were used to test the insecticidal activities of the compounds. Mosquito rearing was carried out in an insectary maintained at 27–28 °C at ca. 80% humidity, on a 12/12 h light/darkness cycle, and maintained at optimal larval concentrations to avoid possible effects of competition. Mosquito larvae were reared in de-chlorinated tap water, and were fed on finely ground Sera Vipan staple diet™ (Sera, Germany), while adults were offered a fresh 10% (w/v) glucose solution meal daily, and were fed on hamster (*Mesocricetus auratus*) as a source of blood meals when egg production was desired. Insecticidal activity tests of the compounds were carried out following the WHO guidelines for testing of adulticides.[67]

For adult mosquito tests, non-blood fed, five day old female mosquitoes were used, and testing was performed in batches of five mosquitoes each. Each batch of mosquitoes was

placed in a 500 ml paper cup and anesthetized by placing the cup in a -20 °C freezer for three minutes. Thereafter, for the topical application tests, the mosquitoes were gently poured onto a plate refrigerated at -20 °C overlaid with a paper towel, and the compound solution (acetone, 0.1 µl) was deposited on the upper part of the pronotum using a micropipetter. As a negative control, 0.1 µl of acetone was applied, while for the positive control, up to 0.1 nmol of propoxur (2-isopropoxyphenyl-*N*-methylcarbamate) in acetone was used.[68]

For the microinjection tests, selected phenoxyacetamide-based inhibitors and propoxur were dissolved in acetone to 100 mM and then diluted in mosquito saline buffer to a total concentration of 5% and 4.3% acetone, respectively. The compound solutions (23 nl; 0.115 nmol and 0.099 nmol of inhibitors and propoxur, respectively) were gently injected into the anesthetized mosquito's intra-thoracic cavities using a Nanoliter2010 Microprocessor controlled nanoliter injector coupled with a Micro4 MicroSyringe Pump Controller (World Precision Instruments). As a negative control, 23 nl of mosquito saline buffer with 5% or 4.3% acetone, respectively, was injected for each experiment. After the respective treatment, the mosquitoes were returned to the insectary, where they were

supplied with a glucose meal and maintained under standard conditions. The mortality rates were recorded after 24 and 48 hours. Mortality rates were adjusted using Abbott's formula[69] in cases where mortality in the control was over 5% and experiments where the mortality in the control were ≥20% were discarded.

ASSOCIATED CONTENT

The Supporting Information is available free of charge on the ACS Publications website at DOI: 10.1021/acs.jmedchem.5b01153.

Synthetic schemes for compounds **11**–**21**, synthetic procedures for compounds **2**–**31**, characterization of synthesized compounds including ^{1}H NMR- and ^{13}C NMR spectra and HRMS data, dose−response curves for compounds **2**–**21**, X-ray crystallography data collection, refinement statistics and detailed descriptions of the binding poses for **15**•*m*AChE (6FSE) and **10**•*m*AChE (6FSD), data of MD simulations: RMSD plots over time, contact plots for **15** and **10** , distance plot between **15** and **S122** in G122S-

*Ag*AChE1, binding poses of **10** in *Ag*AChE1 and raw data of the topical application and microinjection *in vivo* studies.

Smiles data for compounds **1–21** in csv-file.

AUTHOR INFORMATION

Corresponding Author

* Corresponding authors

E-mail address: anna.linusson@umu.se; fredrik.ekstrom@foi.se

Author Contributions

The manuscript was written through contributions of all authors. All authors have given approval to the final version of the manuscript. $ These authors contributed equally.

Funding Sources

The research was funded by the Swedish Research Council (grant numbers: 2014-4218 and 2014-2636).

ACKNOWLEDGMENT

This work was funded by grants from the Swedish Research Council (Dnrs 2014-4218 and 2014-2636) and Centrum for Miljovetenskaplig Forskning (CMF). Students at the Medicinal Chemistry course at Umeå University are acknowledged for their contributions to the synthesis. We are also grateful for excellent technical support at the BESSY II electron storage ring operated by the Helmholtz-Zentrum in Berlin and at the MAX-lab in Lund. The research was conducted on resources provided by the Swedish National Infrastructure for Computing (SNIC) at HPC2N Umeå, Sweden.

ABBREVIATIONS USED

*Aa*AChE1, *Aedes aegypti* acetylcholinesterase 1;

*Ag*AChE1, *Anopheles gambiae* acetylcholinesterase 1;

CAS, catalytic site;

ESP, electrostatic surface potential;

F_c, calculated reflection amplitudes;

F_o, observed reflection amplitudes;

fs, femtosecond;

GAFF, general amber force field;

*h*AChE, *Homo sapiens* acetylcholinesterase;

i.e., *id est* (”that is”);

kJ, kiloJoule;

*m*AChE, *Mus musculus* acetylcholinesterase;

MM/PBSA, molecular mechanics/Poisson-Boltzmann surface area;

n.a., not applicable;

ng, nanograms;

nmol, nanomol;

NPT, number pressure temperature;

ns, nanoseconds;

NVT, number volume temperature;

ps, picosecond;

RESP, restrain electrostatic potential;

SR, selectivity ratio;

WHO, World Health Organization;

STRUCTURAL DATA

Authors will release the atomic coordinates and experimental data of the two crystal structure complexes **15**•*m*AChE (PDB code 6FSE) and **10**•*m*AChE (PDB code 6FSD) upon article publication.

REFERENCES

1. Bhatt, S.; Weiss, D. J.; Cameron, E.; Bisanzio, D.; Mappin, B.; Dalrymple, U.; Battle, K. E.; Moyes, C. L.; Henry, A.; Eckhoff, P. A.; Wenger, E. A.; Briet, O.; Penny, M. A.; Smith, T. A.; Bennett, A.; Yukich, J.; Eisele, T. P.; Griffin, J. T.; Fergus, C. A.; Lynch, M.; Lindgren, F.; Cohen, J. M.; Murray, C. L.; Smith, D. L.; Hay, S. I.; Cibulskis, R. E.; Gething, P. W. The effect of malaria control on *Plasmodium falciparum* in Africa between 2000 and 2015. *Nature* **2015**, *526*, 207-211.

2. WHO World Malaria Report 2016. *Geneva: World Health Organization, 2016* **2016**.

3. Organophosphorus insecticides : a general introduction, Environmental Health Criteria No. 63. World Health Organization, Geneva, 1986, 1-112.

4. Carbamate insecticides : a general introduction, Environmental Health Criteria No. 64. World Health Organization, Geneva, 1986, 1-145.

5. CNN Zika spraying kills millions of honeybees. *Turner Broadcasting System, Inc.* **2016**.

6. Prequalification Vector Control - Prequalified Lists. http://www.who.int/pq-vector-control/prequalified-lists/en/ (accessed 7 June 2018).

7. Toutant, J. P. Insect acetylcholinesterase: catalytic properties, tissue distribution and molecular forms. *Prog. Neurobiol.* **1989**, *32*, 423-446.

8. Weill, M.; Fort, P.; Berthomieu, A.; Dubois, M. P.; Pasteur, N.; Raymond, M. A novel acetylcholinesterase gene in mosquitoes codes for the insecticide target and is non-homologous to the ace gene in *Drosophila*. *Proc. R. Soc. B* **2002**, *269*, 2007-2016.

9. Zhao, P.; Wang, Y.; Jiang, H. Biochemical properties, expression profiles, and tissue localization of orthologous acetylcholinesterase-2 in the mosquito, *Anopheles gambiae*. *Insect Biochem. Mol. Biol.* **2013**, *43*, 260-271.

10. Weill, M.; Lutfalla, G.; Mogensen, K.; Chandre, F.; Berthomieu, A.; Berticat, C.; Pasteur, N.; Philips, A.; Fort, P.; Raymond, M. Comparative genomics: insecticide resistance in mosquito vectors. *Nature* **2003**, *423*, 136-137.

11. Han, Q.; Wong, D. M.; Robinson, H.; Ding, H.; Lam, P. C.; Totrov, M. M.; Carlier, P. R.; Li, J. Crystal structure of acetylcholinesterase catalytic subunits of the malaria vector *Anopheles gambiae*. *Insect Sci.* **2018**, *25*, 721-724.

12. Alout, H.; Berthomieu, A.; Hadjivassilis, A.; Weill, M. A new amino-acid substitution in acetylcholinesterase 1 confers insecticide resistance to *Culex pipiens* mosquitoes from Cyprus. *Insect Biochem. Mol. Biol.* **2007**, *37*, 41-47.

13. Nabeshima, T.; Mori, A.; Kozaki, T.; Iwata, Y.; Hidoh, O.; Harada, S.; Kasai, S.; Severson, D. W.; Kono, Y.; Tomita, T. An amino acid substitution attributable to insecticide-insensitivity of acetylcholinesterase in a Japanese encephalitis vector mosquito, *Culex tritaeniorhynchus*. *Biochem. Biophys. Res. Commun.* **2004**, *313*, 794-801.

14. Cheung, J.; Mahmood, A.; Kalathur, R.; Liu, L.; Carlier, P. R. Structure of the G119S mutant acetylcholinesterase of the malaria vector *Anopheles gambiae* reveals basis of insecticide resistance. *Structure* **2018**, *26*, 130-136.

15. Verma, A.; Wong, D. M.; Islam, R.; Tong, F.; Ghavami, M.; Mutunga, J. M.; Slebodnick, C.; Li, J.; Viayna, E.; Lam, P. C.; Totrov, M. M.; Bloomquist, J. R.; Carlier, P.

R. 3-Oxoisoxazole-2(3H)-carboxamides and isoxazol-3-yl carbamates: resistance-breaking acetylcholinesterase inhibitors targeting the malaria mosquito, *Anopheles gambiae*. *Bioorg. Med. Chem.* **2015**, *23*, 1321-1340.

16. Camerino, E.; Wong, D. M.; Tong, F.; Korber, F.; Gross, A. D.; Islam, R.; Viayna, E.; Mutunga, J. M.; Li, J.; Totrov, M. M.; Bloomquist, J. R.; Carlier, P. R. Difluoromethyl ketones: potent inhibitors of wild type and carbamate-insensitive G119S mutant *Anopheles gambiae* acetylcholinesterase. *Bioorg. Med. Chem. Lett.* **2015**, *25*, 4405-4411.

17. Wong, D. M.; Li, J.; Chen, Q. H.; Han, Q.; Mutunga, J. M.; Wysinski, A.; Anderson, T. D.; Ding, H.; Carpenetti, T. L.; Verma, A.; Islam, R.; Paulson, S. L.; Lam, P. C.; Totrov, M.; Bloomquist, J. R.; Carlier, P. R. Select small core structure carbamates exhibit high contact toxicity to "carbamate-resistant" strain malaria mosquitoes, *Anopheles gambiae* (Akron). *PloS one* **2012**, *7*, e46712.

18. Wong, D. M.; Li, J.; Lam, P. C.; Hartsel, J. A.; Mutunga, J. M.; Totrov, M.; Bloomquist, J. R.; Carlier, P. R. Aryl methylcarbamates: potency and selectivity towards

wild-type and carbamate-insensitive (G119S) *Anopheles gambiae* acetylcholinesterase, and toxicity to G3 strain *An. gambiae*. *Chem.-Biol. Interact.* **2013**, *203*, 314-318.

19. Swale, D. R.; Carlier, P. R.; Hartsel, J. A.; Ma, M.; Bloomquist, J. R. Mosquitocidal carbamates with low toxicity to agricultural pests: an advantageous property for insecticide resistance management. *Pest Manage. Sci.* **2015**, *71*, 1158-1164.

20. Jiang, Y.; Swale, D.; Carlier, P. R.; Hartsel, J. A.; Ma, M.; Ekström, F.; Bloomquist, J. R. Evaluation of novel carbamate insecticides for neurotoxicity to non-target species. *Pestic. Biochem. Physiol.* **2013**, *106*, 156-161.

21. Hartsel, J. A.; Wong, D. M.; Mutunga, J. M.; Ma, M.; Anderson, T. D.; Wysinski, A.; Islam, R.; Wong, E. A.; Paulson, S. L.; Li, J.; Lam, P. C.; Totrov, M. M.; Bloomquist, J. R.; Carlier, P. R. Re-engineering aryl methylcarbamates to confer high selectivity for inhibition of *Anopheles gambiae* versus human acetylcholinesterase. *Bioorg. Med. Chem. Lett.* **2012**, *22*, 4593-4598.

22. Mutunga, J. M.; Chen, Q.-H.; Wong, D. M.; Lam, P. C. H.; Li, J.; Totrov, M. M.; Gross, A. D.; Carlier, P. R.; Bloomquist, J. R. Bivalent carbamates as novel control agents of the malaria mosquito, *Anopheles gambiae*. *Chimia* **2016**, *70*, 704-708.

23. Carlier, P. R.; Anderson, T. D.; Wong, D. M.; Hsu, D. C.; Hartsel, J.; Ma, M.; Wong, E. A.; Choudhury, R.; Lam, P. C.; Totrov, M. M.; Bloomquist, J. R. Towards a species-selective acetylcholinesterase inhibitor to control the mosquito vector of malaria, *Anopheles gambiae*. *Chem.-Biol. Interact.* **2008**, *175*, 368-375.

24. Dou, D.; Park, J. G.; Rana, S.; Madden, B. J.; Jiang, H.; Pang, Y. P. Novel selective and irreversible mosquito acetylcholinesterase inhibitors for controlling malaria and other mosquito-borne diseases. *Sci. Rep.* **2013**, *3*, 1068.

25. Pang, Y. P. Novel acetylcholinesterase target site for malaria mosquito control. *PloS one* **2006**, *1*, e58.

26. Pang, Y. P. Species marker for developing novel and safe pesticides. *Bioorg. Med. Chem. Lett.* **2007**, *17*, 197-199.

27. Pang, Y. P.; Brimijoin, S.; Ragsdale, D. W.; Zhu, K. Y.; Suranyi, R. Novel and viable acetylcholinesterase target site for developing effective and environmentally safe insecticides. *Curr. Drug Targets* **2012**, *13*, 471-482.

28. Pang, Y. P.; Ekström, F.; Polsinelli, G. A.; Gao, Y.; Rana, S.; Hua, D. H.; Andersson, B.; Andersson, P. O.; Peng, L.; Singh, S. K.; Mishra, R. K.; Zhu, K. Y.; Fallon,

A. M.; Ragsdale, D. W.; Brimijoin, S. Selective and irreversible inhibitors of mosquito acetylcholinesterases for controlling malaria and other mosquito-borne diseases. *PloS one* **2009**, *4*, e6851.

29. Engdahl, C.; Knutsson, S.; Ekström, F.; Linusson, A. Discovery of selective inhibitors targeting acetylcholinesterase 1 from disease-transmitting mosquitoes. *J. Med. Chem.* **2016**, *59*, 9409-9421.

30. Knutsson, S.; Kindahl, T.; Engdahl, C.; Nikjoo, D.; Forsgren, N.; Kitur, S.; Ekström, F.; Kamau, L.; Linusson, A. N-Aryl-N'-ethyleneaminothioureas effectively inhibit acetylcholinesterase 1 from disease-transmitting mosquitoes. *Eur. J. Med. Chem.* **2017**, *134*, 415-427.

31. Engdahl, C.; Knutsson, S.; Fredriksson, S. A.; Linusson, A.; Bucht, G.; Ekström, F. Acetylcholinesterases from the disease vectors *Aedes aegypti* and *Anopheles gambiae*: Functional characterization and comparisons with vertebrate orthologues. *PloS one* **2015**, *10*, e0138598.

32. Alout, H.; Labbe, P.; Berthomieu, A.; Djogbenou, L.; Leonetti, J. P.; Fort, P.; Weill, M. Novel AChE inhibitors for sustainable insecticide resistance management. *PloS one* **2012**, *7*, e47125.

33. Kryger, G.; Silman, I.; Sussman, J. L. Structure of acetylcholinesterase complexed with E2020 (Aricept (R)): implications for the design of new anti-Alzheimer drugs. *Structure* **1999**, *7*, 297-307.

34. Berg, L.; Mishra, B. K.; Andersson, C. D.; Ekström, F.; Linusson, A. The nature of activated non-classical hydrogen bonds: a case study on acetylcholinesterase-ligand complexes. *Chem. - Eur. J.* **2016**, *22*, 2672-2681.

35. Nuss, A. B.; Ejendal, K. F.; Doyle, T. B.; Meyer, J. M.; Lang, E. G.; Watts, V. J.; Hill, C. A. Dopamine receptor antagonists as new mode-of-action insecticide leads for control of *Aedes* and *Culex* mosquito vectors. *PLoS Neglected Trop. Dis.* **2015**, *9*, e0003515.

36. Tice, C. M. Selecting the right compounds for screening: Does Lipinski's Rule of 5 for pharmaceuticals apply to agrochemicals? *Pest Manage. Sci.* **2001**, *57*, 3-16.

37. Turner, J. A.; Ruscoe, C. N.; Perrior, T. R. Discovery to development: insecticides for malaria vector control. *Chimia* **2016**, *70*, 684-693.

38. Hao, G.; Dong, Q.; Yang, G. A comparative study on the constitutive properties of marketed pesticides. *Mol. Inf.* **2011**, *30*, 614-622.

39. Clarke, E. D.; Delaney, J. S. Physical and molecular properties of agrochemicals: an analysis of screen inputs, hits, leads, and products. *Chimia* **2003**, *57*, 731-734.

40. Artursson, E.; Akfur, C.; Hörnberg, A.; Worek, F.; Ekström, F. Reactivation of tabun-*h*AChE investigated by structurally analogous oximes and mutagenesis. *Toxicology* **2009**, *265*, 108-114.

41. Ellman, G. L.; Courtney, K. D.; Andres, V., Jr.; Feather-Stone, R. M. A new and rapid colorimetric determination of acetylcholinesterase activity. *Biochem. Pharmacol.* **1961**, *7*, 88-95.

42. *version 6.04 for Windows, GraphPad Software, La Jolla California USA, www.graphpad.com*, 2014

43. Ekström, F.; Akfur, C.; Tunemalm, A. K.; Lundberg, S. Structural changes of phenylalanine 338 and histidine 447 revealed by the crystal structures of tabun-inhibited murine acetylcholinesterase. *Biochemistry* **2006**, *45*, 74-81.

44. Kabsch, W. Automatic processing of rotation diffraction data from crystals of initially unknown symmetry and cell constants *J. Appl. Crystallogr.* **1993**, *26*, 795-800.

45. Murshudov, G. N.; Vagin, A. A.; Dodson, E. J. Refinement of macromolecular structures by the maximum-likelihood method. *Acta Crystallogr., Sect. D: Biol. Crystallogr.* **1997**, *53*, 240-255.

46. Bourne, Y.; Taylor, P.; Radic, Z.; Marchot, P. Structural insights into ligand interactions at the acetylcholinesterase peripheral anionic site. *EMBO J.* **2003**, *22*, 1-12.

47. Adams, P. D.; Grosse-Kunstleve, R. W.; Hung, L. W.; Ioerger, T. R.; McCoy, A. J.; Moriarty, N. W.; Read, R. J.; Sacchettini, J. C.; Sauter, N. K.; Terwilliger, T. C. PHENIX: building new software for automated crystallographic structure determination. *Acta Crystallogr., Sect. D: Biol. Crystallogr.* **2002**, *58*, 1948-1954.

48. Emsley, P.; Cowtan, K. Coot: model-building tools for molecular graphics. *Acta Crystallogr., Sect. D: Biol. Crystallogr.* **2004**, *60*, 2126-2132.

49. Sievers, F.; Wilm, A.; Dineen, D.; Gibson, T. J.; Karplus, K.; Li, W. Z.; Lopez, R.; McWilliam, H.; Remmert, M.; Soding, J.; Thompson, J. D.; Higgins, D. G. Fast, scalable generation of high-quality protein multiple sequence alignments using Clustal Omega. *Mol. Syst. Biol.* **2011**, *7*, Article number 539.

50. Sali, A.; Blundell, T. L. Comparative protein modeling by satisfaction of spatial restraints. *J. Mol. Biol.* **1993**, *234*, 779-815.

51. O'Boyle, N. M.; Banck, M.; James, C. A.; Morley, C.; Vandermeersch, T.; Hutchison, G. R. Open Babel: an open chemical toolbox. *J. Cheminf.* **2011**, *3*, 33.

52. Frisch, M.; Trucks, G.; Schlegel, H. B.; Scuseria, G.; Robb, M.; Cheeseman, J.; Scalmani, G.; Barone, V.; Mennucci, B.; Petersson, G. Gaussian 09, Revision A. 02, Gaussian. *Inc., Wallingford, CT* **2009**, *200*.

53. *AMBER*, University of California: San Francisco, 2017.

54. Wang, J.; Wolf, R. M.; Caldwell, J. W.; Kollman, P. A.; Case, D. A. Development and testing of a general amber force field. *J. Comput. Chem.* **2004**, *25*, 1157-1174.

55. Sousa da Silva, A. W.; Vranken, W. F. ACPYPE - AnteChamber PYthon Parser interfacE. *BMC Res. Notes* **2012**, *5*, 367.

56. Lindorff-Larsen, K.; Piana, S.; Palmo, K.; Maragakis, P.; Klepeis, J. L.; Dror, R. O.; Shaw, D. E. Improved side-chain torsion potentials for the Amber ff99SB protein force field. *Proteins* **2010**, *78*, 1950-1958.

57. Pronk, S.; Pall, S.; Schulz, R.; Larsson, P.; Bjelkmar, P.; Apostolov, R.; Shirts, M. R.; Smith, J. C.; Kasson, P. M.; van der Spoel, D.; Hess, B.; Lindahl, E. GROMACS 4.5: a high-throughput and highly parallel open source molecular simulation toolkit. *Bioinformatics* **2013**, *29*, 845-854.

58. Jorgensen, W. L.; Chandrasekhar, J.; Madura, J. D.; Impey, R. W.; Klein, M. L. Comparison of simple potential functions for simulating liquid water. *J. Chem. Phys.* **1983**, *79*, 926-935.

59. Berendsen, H. J. C.; Postma, J. P. M.; Vangunsteren, W. F.; Dinola, A.; Haak, J. R. Molecular-dynamics with coupling to an external bath. *J. Chem. Phys.* **1984**, *81*, 3684-3690.

60. Bussi, G.; Donadio, D.; Parrinello, M. Canonical sampling through velocity rescaling. *J. Chem. Phys.* **2007**, *126*, Article number 014101.

61. Nose, S.; Klein, M. L. Constant pressure molecular-dynamics for molecular-systems. *Mol. Phys.* **1983**, *50*, 1055-1076.

62. Darden, T.; York, D.; Pedersen, L. Particle Mesh Ewald - an N.Log(N) method for Ewald sums in large systems. *J. Chem. Phys.* **1993**, *98*, 10089-10092.

63. Hess, B. P-LINCS: a parallel linear constraint solver for molecular simulation. *J. Chem. Theory Comput.* **2008**, *4*, 116-122.

64. Hess, B.; Bekker, H.; Berendsen, H. J. C.; Fraaije, J. G. E. M. LINCS: a linear constraint solver for molecular simulations. *J. Comput. Chem.* **1997**, *18*, 1463-1472.

65. Kumari, R.; Kumar, R.; Lynn, A. g_mmpbsa--a GROMACS tool for high-throughput MM-PBSA calculations. *J. Chem. Inf. Model.* **2014**, *54*, 1951-1962.

66. Gohlke, H.; Kiel, C.; Case, D. A. Insights into protein-protein binding by binding free energy calculation and free energy decomposition for the Ras-Raf and Ras-RalGDS complexes. *J. Mol. Biol.* **2003**, *330*, 891-913.

67. WHO Guidelines for laboratory and field testing of mosquito larvicides. *WHO/CDS/NTD/WHOPES/GCDPP/2005.13* **2005**.

68. Bonnet, J.; Pennetier, C.; Duchon, S.; Lapied, B.; Corbel, V. Multi-function oxidases are responsible for the synergistic interactions occurring between repellents and insecticides in mosquitoes. *Parasites Vectors* **2009**, *2*, 17.

69. Abbott, W. S. A method of computing the effectiveness of an insecticide. 1925. *J. Am. Mosq. Control Assoc.* **1987**, *3*, 302-303.

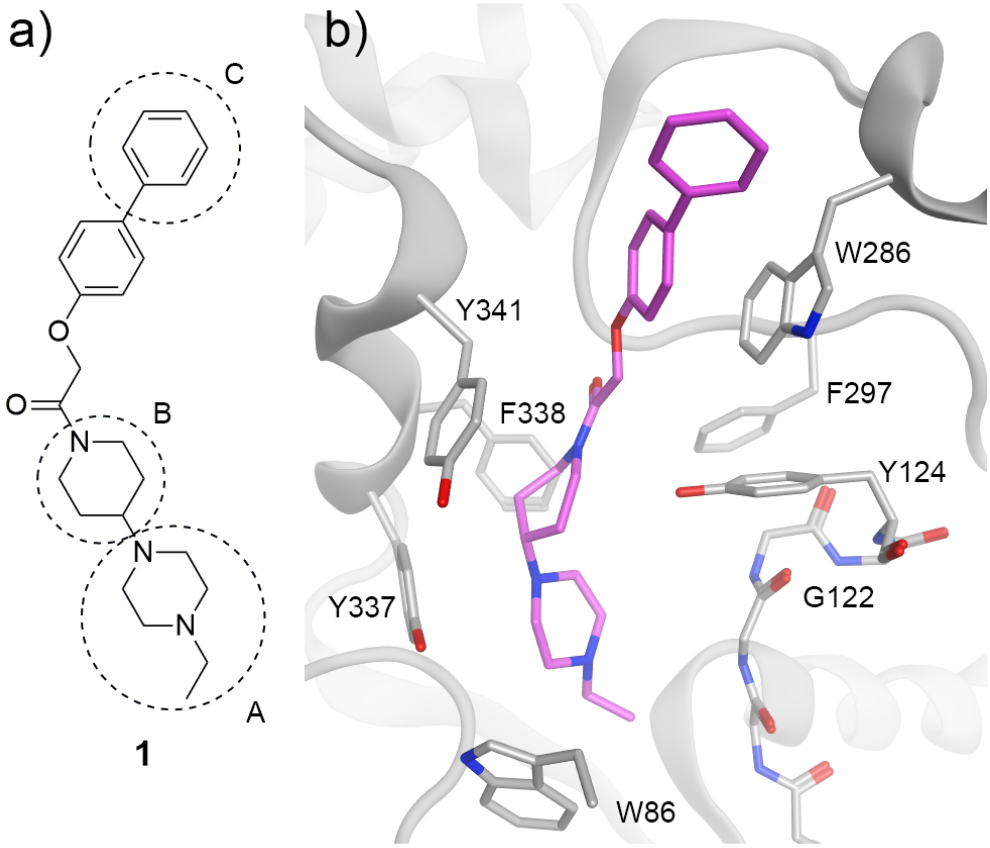

Figure 1. The chemical structure of 1 (a) and the binding pose of 1 in mAChE (b).28 Three elements (A, B and C) of the parent molecule were varied in the design of analogues. Amino acid residues of mAChE that form the active site gorge are highlighted.

83x75mm (300 x 300 DPI)

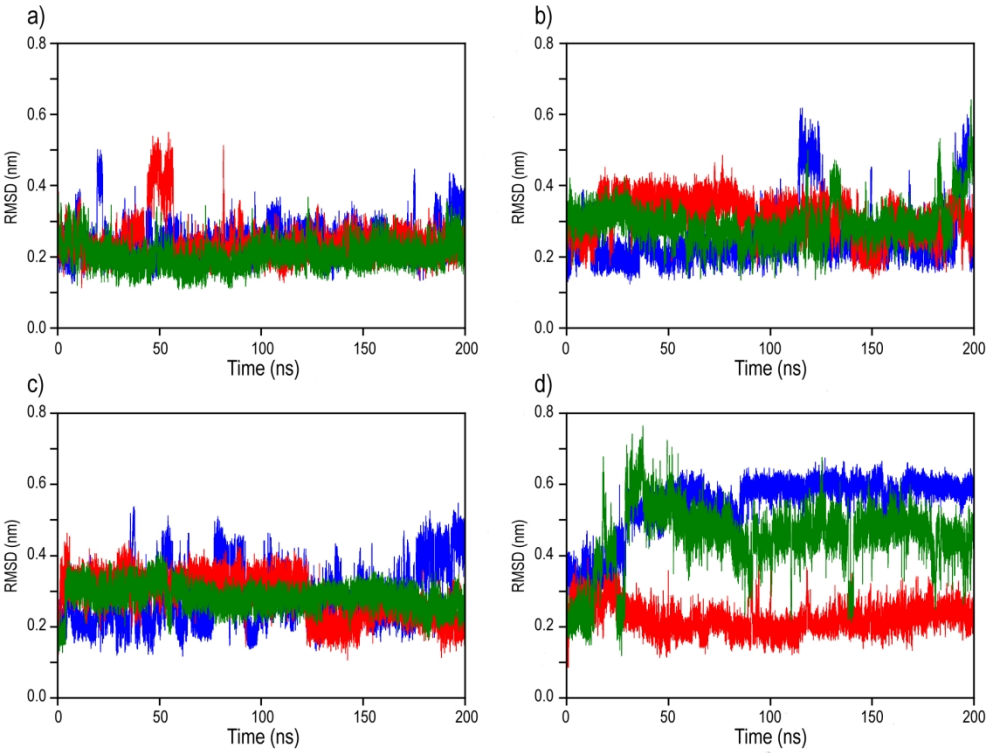

Figure 2. The dynamics over time of compound 15 in complex with a) AaAChE1, b) AgAChE1, c) G122S-AgAChE1, and d) mAChE according to its RMSD after superimposing the enzyme backbone; blue, red, and green curves correspond to simulations S1, S2, and S3, respectively.

166x126mm (300 x 300 DPI)

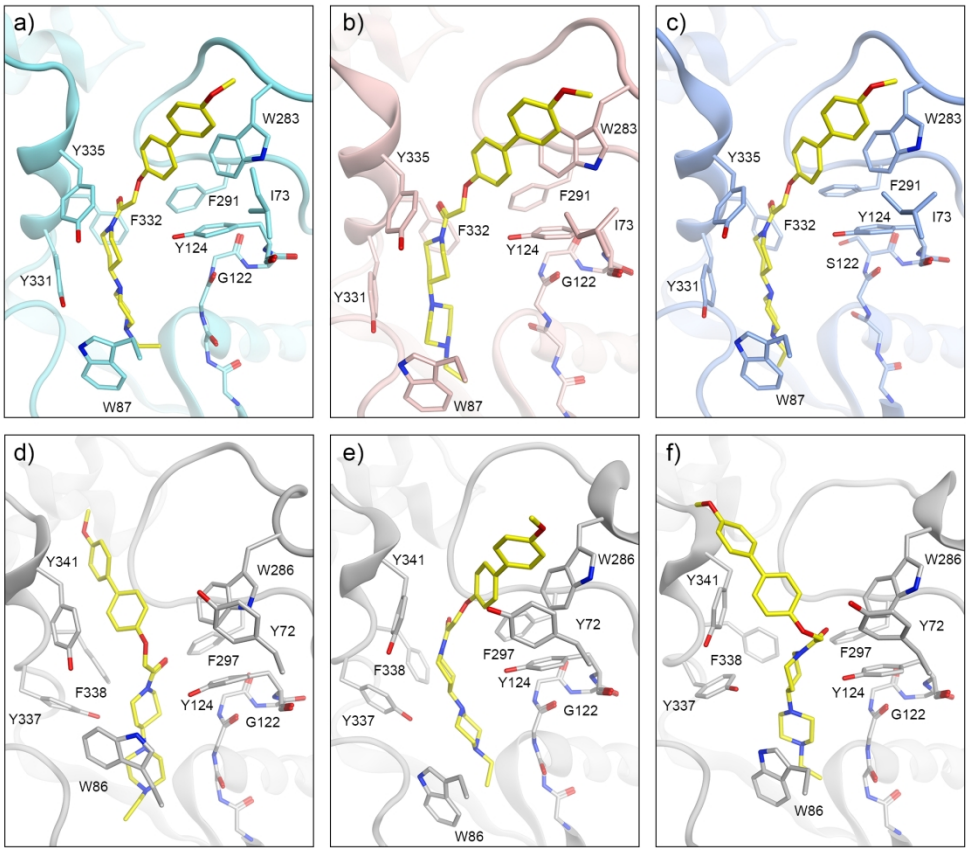

Figure 3. Binding poses of 15 in AChEs based on MD simulations. The poses were extracted from the most populated conformations of 15 (yellow) during the MD simulations of the mosquito enzymes AaAChE1 (a, cyan), AgAChE1 (b, pink), and G122S-AgAChE1 (c, blue). The three most populated conformations of 15 in the mouse enzyme (grey) are shown in d–f, where e is most similar to the crystal structure of 15•mAChE.

175x155mm (300 x 300 DPI)

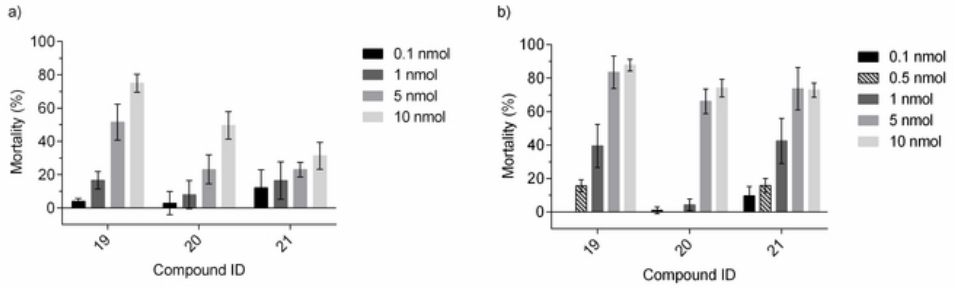

Figure 4. The intrinsic insecticidal efficacy of compound 19-21 recorded 24 hours after topical application on adult female Ae. aegypti (a) and An. gambiae (b) mosquitoes.

58x19mm (300 x 300 DPI)

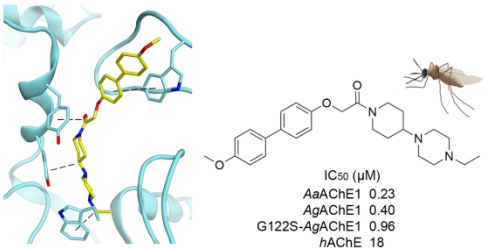

Table of Contents Figure

209x55mm (300 x 300 DPI)